Analyst

Cite this: *Analyst*, 2012, **137**, 1031

www.rsc.org/analyst

PAPER

Morphology controllable synthesis of monkshoodvine root-bark like carbon and its biosensing application

Yaping He, Jianbin Zheng* and Qinglin Sheng

Received 31st October 2011, Accepted 1st December 2011
DOI: 10.1039/c2an16032c

Unique monkshoodvine root–bark like morphology carbon materials (MLC) have been successfully synthesized under hydrothermal conditions. Utilizing the merits of high surface area and good electron conductivity of the MLC, a layered biosensor designed by assembling the MLC, hemoglobin (Hb) and gold nanoparticles was further developed. Scanning electron microscope and transmission electron microscope showed that the morphology of carbon materials can be successfully controlled simply by moderating the initiator amount of precursor and reaction temperature. The results indicated that the MLC was formed at the reaction condition of 5 mg Ferrocene + 6 mL CCl_4 at 280 °C. Electrochemical methods, such as cyclic voltammetry and electrochemical impedance spectroscopy, were used to characterize the layered biosensor and its application for sensitive detection of hydrogen peroxide (H_2O_2). Under optimized experimental condition, the linear range for the determination of H_2O_2 was 0.06 μM to 1.6 mM with a detection limit of 0.03 μM (S/N = 3). Furthermore, the biosensor also showed a fast response (within 2 s) and high stability.

1. Introduction

Dimensionality plays an important role in determining properties of nanomaterials and synthesis of nanostructures with controllable morphology, size, chemical composition and crystal orientation.[1] The unique dimensionalities and structures of carbon nanomaterials (CNMs) endow them with the properties of good catalysis ability and high conductivity. CNMs can enhance the electrochemical reactivity of important biomolecules and promote their electron transfer ability.[2] The CNMs have attracted a great deal of interest since the discovery of carbon nanotubes (CNTs) in 1991.[3] CNMs of different structure such as bamboo-shape carbon,[4] yarn-like carbon fiber,[5] sea urchin-like carbon,[6] cup-shaped nanocarbon[7] and core/shell composite nanowires[8] have been successfully prepared. Some of them have been applied to the construction of novel biosensors. Carbon spheres were used to fabricate hydrogen peroxide (H_2O_2) biosensor.[9] Three dimensional ordered graphitized mesoporous carbon GMC-6 (pore diameter 6 nm) and GMC-13 (pore diameter 13 nm) were employed systematically for the construction of enzyme-based electrochemical biosensors.[10] Graphene was employed to prepare glucose and H_2O_2 biosensor.[11,12] Single-walled carbon nanohorns have been widely studied for various biosensors.[13] Multi-walled carbon nanotubes were employed as the carriers of the electrochemical capture probe to develop a novel electrochemical aptamer sensor for thrombin detection.[14] The high sensitivity and conductivity of CNMs to surface adsorbents promote the application of CNMs as highly sensitive nanoscale sensors[15] from amperometric enzyme electrodes to DNA hybridization biosensors.

In order to fabricate more high quality sensors based on CNMs, it is necessary to develop some novel types of CNMs and widen their application in biosensors. The novel morphology monkshoodvine root-bark like carbon (MLC) was controllably synthesized by our group, which is described in the Experimental section. The morphology of the MLC is cylindrical stem with porous on the surface and leaf blade pinnately veined just as the plant monkshoodvine root-bark. The MLC offers more efficient ways for electron transfer between sensor electrodes and the redox-active sites of biological molecules, which are frequently embedded inside surrounding peptides. It proved to be good conductivity and high biocompatibility. Besides that, large surface areas of the MLC make a stable and effective immobilization of biomolecules on the electrode surface, which is always a crucial aspect for the preparation of biosensors.[16,17]

Gold nanoparticles (AuNPs) provide an environment similar to redox proteins and afford the protein molecules more freedom for orientation. Thus, AuNPs reduce the insulating property of the protein shell for the direct electron transfer and facilitate the electron transfer through the conducting tunnels of colloidal gold.[18] It offers a stable immobilization of biomolecules to retain their bioactivity, which is a major advantage for the preparation of biosensors.[19] The properties of the new kind of CNMs will be optimized by the combination of AuNPs. Poly(diallyldimethylammonium chloride) (PDDA) can induce the

Institute of Analytical Science/Shaanxi Provincial Key Laboratory of Electroanalytical Chemistry, Northwest University, Xi'an, Shaanxi, 710069, China. E-mail: zhengjb@nwu.edu.cn; Fax: +86 29 88303448; Tel: +86 29 88303448

aggregation of the molecule with opposite charge and a new combination can be formed.[20] Herein, the MLC can evenly disperse and form a positively charged composite PDDA–MLC, which is convenient for next assembly.

The aim of the present work is to controllably synthesize the MLC and employ it to fabricate a H_2O_2 biosensor by layer-by-layer assembly of hemoglobin (Hb) and PDDA–MLC/AuNPs onto an *O*-phenylenediamine (PDA) modified electrode. The electrochemical and eletrocatalytic behaviors of Hb in the new system are also studied.

2. Experimental

2.1. Apparatus and measurements

Fourier transform infrared spectra (FTIR) were recorded on KBr disk using a Nicolet 380 FTIR spectrometer (Thermo Electron Corporation, USA). UV-vis spectra were obtained on a Cary 50 probe UV-vis spectrophotometer (Varian, Australia). Jeol Neoscope Benchtop scanning electron microscope (SEM) was used for SEM images (JEOL, Japan). Transmission electron microscope (TEM) image was collected on an E.M. 912 Ω energy-filtering TEM (120 kV) (JEOL, Japan). All electrochemical experiments were carried out on a CHI 660D electrochemical workstation (Shanghai CH Instrument Co. Ltd., China) using a three electrode system. Indium oxide glass (ITO; Hebei Lingxian Gaoke Co. Ltd.) was used as a substrate for assembly of multilayer films and was cleaned by sonicate treatment sequentially for 20 min in acetone, 10% KOH in ethanol and distilled water.[21] The working electrode was ITO or modified ITO electrode. A saturated calomel electrode (SCE) and a platinum electrode were served as reference and counter electrodes, respectively. All tested solutions were purged with highly purified nitrogen for 30 min before experiments and a nitrogen environment was kept over the solution during electrochemical measurements.

2.2. Reagents

Bovine hemoglobin (Hb, MW. 64500, Sigma Company), Chloroauricacid tetrahydrate ($HAuCl_4 \cdot 4H_2O$) were supplied by Sigma. PDDA (20%, MW. 200000–350000) was obtained from Aldrich. PDA was obtained from Shanghai Shanpu Chemical Co. Ltd. (Shanghai, China), chitosan (CHIT, MW. 5–6 × 10^5, >90% deacetylation) was purchased from Shanghai Yuanju Biotechnology Co., Ltd (Shanghai, China). Ferrocene (Fc, 97%, Aldrich), H_2O_2 (w/w, 30%) was obtained from Tianjin TianLi Chemical Reagent Ltd (Tianjin, China). Other reagents were analytical reagent grade and doubly distilled water was used in all the experiments. 0.1 M sodium phosphate buffered saline (PBS) with various pH values was prepared by mixing stock standard solutions of Na_2HPO_4 and KH_2PO_4 and adjusting the pH with 0.1 M H_3PO_4 or NaOH. All the electrochemical experiments were conducted at room temperature (25 ± 2 °C).

2.3. Preparation of Hb/{PDDA–MLC/AuNPs}$_n$ multilayer film

2.3.1. Preparation of AuNPs. AuNPs were prepared based on a previous report[22] as follows: 1 mL of $HAuCl_4$ solution (w/w, 1%) was added into 100 mL flask, then heated until the solution to be boiling, 5 mL of sodium citrate solution (w/w, 1%) was quickly added while stirring vigorously. After continuous boiling for 30 min, it was allowed to cool down. The negatively charged AuNPs were prepared.

2.3.2. Preparation of the MLC. The MLC was prepared by a simple hydrothermal method. In a typical synthesis, 5 mg of Fc powder was mixed with 6 mL carbon tetrachloride (CCl_4) solution followed by hydrothermal treatment of the mixture at 280 °C in a 10 mL teflon-lined autoclave for 24 h. After reaction, the black precipitate was separated by filtration, washed with absolute ethanol and distilled water until the impurities were all removed. Then the black sample was dried in a vacuum oven at 50 °C for 24 h, the MLC was prepared.

2.3.3. Preparation of Hb/{PDDA–MLC/AuNPs}$_n$ film. The assembly process of Hb/{PDDA–MLC/AuNPs}$_n$ film followed: (1) PDA was electropolymerized[20] onto the ITO electrode surface by cycling the potential between −0.25 and 0.8 V (*vs.* SCE) in 10 mL of 0.1 M pH 6.0 PBS containing 10 mM PDA and 25 mM KCl for 20 consecutive scans. The treated substrate electrode was washed with distilled water. (2) After drying, dipped it into the negatively charged AuNPs and positively charged the PDDA–MLC aqueous solution (1 mg MLC in w/w 5% PDDA containing 0.1 M NaCl) for 30 min, respectively. Layer-by-layer assembly films of AuNPs and PDDA–MLC were fabricated by alternately immersing the electrode with precursor film. (3) The {PDDA–MLC/AuNPs}$_n$/PDA/ITO electrode was immersed into Hb (5 mg mL^{-1} in pH 8.0 PBS) 4 °C for 12 h. The proposed modified electrode was denominated as Hb/{PDDA–MLC/AuNPs}$_n$/PDA/ITO. The biosensor was stored at 4 °C when not in use.

3. Results and discussion

3.1. Synthesis and characterization of the MLC

The morphology of the MLC was observed by SEM and TEM. Fig. 1A is a photograph of the plant monkshoodvine root-bark. As it is shown, monkshoodvine root-bark is a cylindrical stem with lenticels and leaf blade pinnately veined. The products at the reaction condition of 5 mg Fc + 6 mL CCl_4 at 280 °C (as shown in Fig. 1B) were quite similar to that. The width of the leaf ranged from 0.3 to 0.6 μm and the length of the leaf blade was 1 to 3 μm. The rough surface with porous structure is beneficial for effective immobilization of enzyme, protein and other bioactive substances.

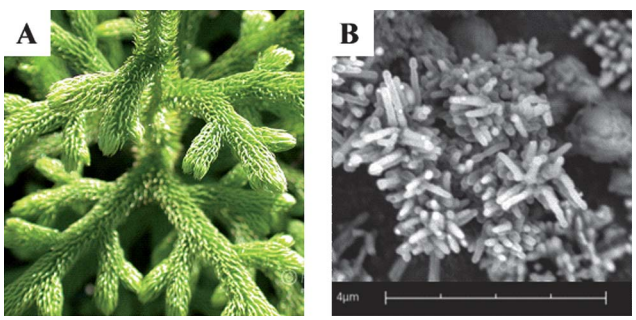

Fig. 1 (A) Photograph of the plant monkshoodvine root-bark; (B) SEM images of the MLC.

In order to further study the possible formation mechanism of the MLC, a series of controllable hydrothermal experiments were made in 10 mL teflon-lined autoclave. (i) The reaction condition was set at 5 mg Fc + 6 mL CCl_4 at 240 °C for 24 h. SEM imagine (Fig. 2A) analysis indicated that the resulting products primarily consisted of even distributed carbon microsphere of diameter 3 to 5 μm with an open mouth, and each microsphere has a deep notch at the open mouth. (ii) The reaction occurred at 5 mg Fc + 6 mL CCl_4 at 260 °C for 24 h. It was found that the products were a mixture of carbon microspheres with a decreased diameter and some MLC, as shown in Fig. 2B. (iii) The reaction condition was set at 2.5 mg Fc + 6 mL CCl_4 at 280 °C for 24 h. TEM image (Fig. 2C) analysis indicated that the resulting products primarily consisted of tripod shaped carbon with an open mouth at the terminal. (iv) The reaction condition was set at 2 mg Fc + 6 mL CCl_4 at 280 °C for 24 h. Volume comb shape carbon is shown (Fig. 2D). (v) The reaction condition was set at 10 mg Fc + 6 mL CCl_4 at 280 °C for 24 h. A big carbon sphere with small carbon sphere array on the surface was obtained, as shown in Fig. 2E.

The above observations were intriguing and a possible self-seeded surface-deposition growth mechanism is proposed based on experimental facts and depicted in Scheme 1. As we known, cyclopentadienyl groups[23] and CCl_4[24] had been employed for the formation of CNMs. Here, Fc and CCl_4 were also used for the formation of the MLC under mild solvothermal conditions. Organometallic complexes Fc act both as a catalyst and a carbon source to form the shaped carbon materials.[25] The growth process should be divided into two parts: (I) the formation of carbon nanoparticles (CNPs) and Fe(II) the formation of different shaped CNMs. As shown in Scheme 1. I, hydrothermal synthesis led to the decomposition of Fc[26] to form Fe(II) and cyclopentadienyl groups. Fe(II) can react with CCl_4 (reaction b) to form Fe(III) and small inhomogeneous CNPs.

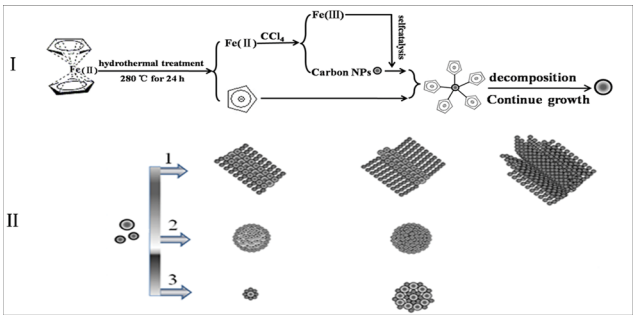

Scheme 1 The possible formation mechanism of monkshoodvine root-bark like carbon.

Cyclopentadienyl groups can be immobilized at the surfaces of CNPs under the Fe(III) severing as catalyst through dehydrogenization and bonding process (reaction d). Small inhomogeneous carbon nanospheres were formed, under the repeat decomposition of Fc and the continuous growth of cyclopentadienyl groups onto CNPs.

Then, as also shown in Scheme 1. II, there may be three possible way to form the shaped carbon materials: (1) The bigger carbon nanospheres are arrayed and coalesce to form an axis. The smaller carbon nanospheres coalesce with the bigger ones and vertical grow one by one to form a zigzag carbon tube on the axis. This process formed volume comb shape carbon. With the continuous growing of the smaller carbon nanospheres, the MLC was formed. At very low initiator amount of precursor, tripod shaped carbon was obtained. (2) The bigger carbon nanospheres agglomerate to form a nucleus, and the smaller nanospheres homogeneously grow on the nucleus to form bigger carbon spheres with an open mouth at the terminal. This process mainly occurred at relatively lower

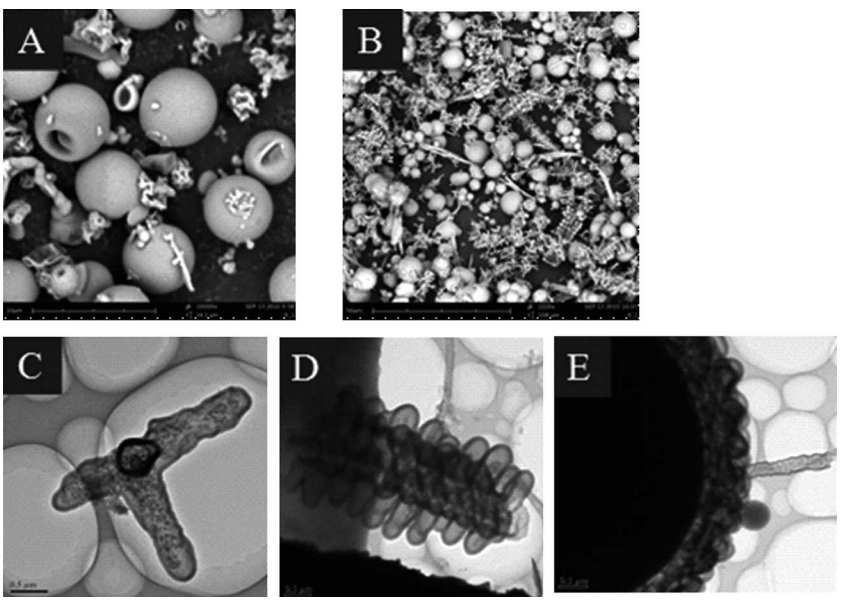

Fig. 2 (A) SEM images of the products at the reaction condition of 5 mg Fc + 6 mL CCl_4 at 240 °C; (B) SEM images of the products at the reaction condition of 5 mg Fc + 6 mL CCl_4 at 260 °C; (C) TEM images of the products at the reaction condition of 2.5 mg Fc + 6 mL CCl_4 at 280 °C; (D) TEM images of the products at the reaction condition of 2 mg Fc + 6 mL CCl_4 at 280 °C; (E) TEM images of the products at the reaction condition of 10 mg Fc + 6 mL CCl_4 at 280 °C.

temperature. With the increase of temperature, the mass movement was aggravated. Heterogeneous effect makes the growth of the smaller carbon nanosphere coalesce with the bigger ones and vertically grow one by one to form a zigzag carbon tube on the formed carbon sphere. The products are a mixture of carbon microsphere and the MLC. (3) A bigger carbon nanosphere as a nucleus, the smaller nanospheres homogeneous agglomerate on it, then, the bigger carbon nanospheres homogeneous agglomerate on the smaller nanospheres, this process repeated. Big carbon spheres with the smaller carbon sphere array on the surface was obtained. This process mainly occurred at the high initiator amount of precursor. Although the temperature is high enough, the heterogeneous effect is hindered by the mass movement. A specific phenomenon happened. The bigger nanospheres agglomerate, the smaller nanospheres go into the interstice.

N_2 isothermal was used to confirm the presence of porous structure in the MLC. As shown in Fig. 3A, according to classification standard of IUPAC (International Union of Pure and Applied Chemistry), adsorptive isothermal of the MLC was the second kind. When the relative pressure gets to 1, the adsorption capacity are far away from saturation, which suggested that there are porous structures in the MLC.

FTIR was also used to monitor the structure conformations of the MLC, as shown in Fig. 3B. The absorbance at 3422.5 cm^{-1} was ascribed to the stretching vibration of –OH of the carboxyl group. The absorbance at 1712.7 cm^{-1} was due to the C=O stretch of the carboxyl group. The band at the 1544.3 cm^{-1} corresponds to the stretching mode of the C=C double bond that forms the framework of the carbon nanotube sidewall. All the above indicated that the prepared the MLC had carboxyl group, which is convenient for the development of biosensors.

3.2. Influence of assembly layers

The evidence of multilayer growth of Hb/{MLC-PDDA/AuNPs}$_n$/PDA was observed *via* electrochemical method. Ferricyanide was chosen as a marker to investigate the change of electrode behavior after each assembly step. As shown in Fig. 4A, with the treatment of PDA, no peak was observed at the bare ITO (curve a) in the solution of 1.0 mM $[Fe(CN)_6]^{3-}$ + 0.1 M KCl as the supporting electrolyte, indicating successful electropolymerization of PDA. The {PDDA–MLC/AuNPs}/PDA/ITO (curve c), the {PDDA–MLC/AuNPs}$_2$/PDA/ITO (curve d) and the {PDDA–MLC/AuNPs}$_3$/PDA/ITO (curve e) had much bigger peak current than that of the bare ITO electrode (curve b) and larger background currents, indicating that the effectively electroactive area of the ITO increased. However, the peak currents did not increase after four layers or even more layers assembly of the PDDA–MLC/AuNPs. All the above illustrated that the optimal assembly layer number of the PDDA–MLC/AuNPs film was three. The electron transfer was enhanced and mainly contributed to the MLC with good conductivity and unique spatial trends. The {PDDA–MLC/AuNPs}$_3$/PDA/ITO could provide a favorable microenvironment for bioactive substances to retain their natural structures. Because of the good conductivity and unique of spatial trends, the MLC could improve the rate of the electron transfer and the immobilization of enzyme and it will be distinctive in practical applications.

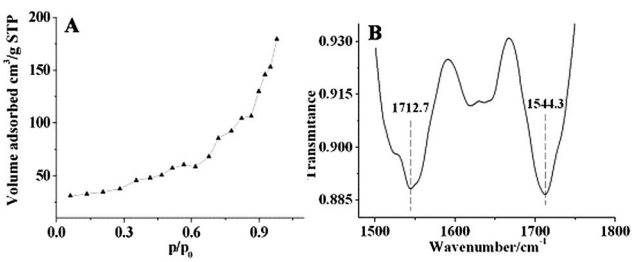

Fig. 3 (A) N_2 adsorption isotherms of the MLC; (B) FTIR spectra of the MLC.

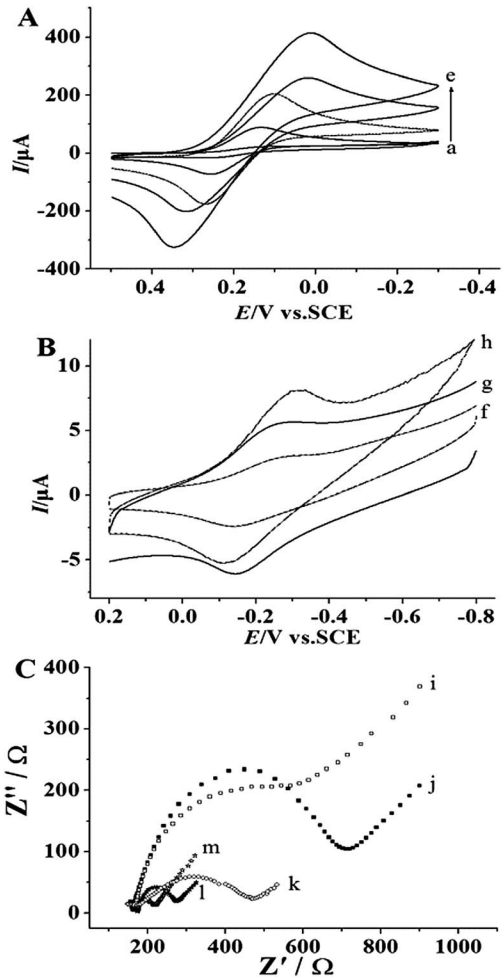

Fig. 4 (A) Cyclic voltammograms (CVs) of the PDA/ITO (a), the bare ITO (b), the {PDDA–MLC/AuNPs}/PDA/ITO (c), the {PDDA–MLC/AuNPs}$_2$/PDA/ITO (d) and the {PDDA–MLC/AuNPs}$_3$/PDA/ITO (e) in a solution of 1 mM $[Fe(CN)_6]^{3-}$ + 0.1 M KCl as the supporting electrolyte at scan rate of 100 mV s^{-1}. (B) CVs of the Hb/{PDDA–MLC/AuNPs}/PDA/ITO (f), the Hb/{PDDA–MLC/AuNPs}$_2$/PDA/ITO (g) and the Hb/{PDDA–MLC/AuNPs}$_3$/PDA/ITO (h) in N_2-saturated PBS at the scan rate of 100 mV s^{-1}. (C) EIS plots for the bare ITO (i), the PDA/ITO (j), the {PDDA–MLC/AuNPs}/PDA/ITO (k), the {PDDA–MLC/AuNPs}$_2$/PDA/ITO (l) and the {PDDA–MLC/AuNPs}$_3$/PDA/ITO (m) in a solution of 1 mM $[Fe(CN)_6]^{3-/4-}$ + 0.1 M KCl as the supporting electrolyte. The frequencies swept from 10^5 to 10^{-2} Hz.

The influence of assembly layers by the electrochemical response of Hb in the N_2-saturated 0.1 M pH 7.0 PBS was further investigated. The Hb/{PDDA–MLC/AuNPs}/PDA/ITO showed a pair of well-defined, quasi-reversible redox peaks with the scan rate of 100 mV s^{-1}, as shown in Fig. 4B, curve f. Under the same condition, the Hb/{PDDA–MLC/AuNPs}$_2$/PDA/ITO (Fig. 4B, curve g) and the Hb/{PDDA–MLC/AuNPs}$_3$/PDA/ITO (Fig. 4B, curve h) showed a pair of well-defined, quasi-reversible redox peaks with increasing peak currents and larger background currents, which were in good agreement with the results of the cyclic voltammograms (CVs) of ferricyanide mentioned above. The biosensor based on the Hb/{PDDA–MLC/AuNPs}$_3$/PDA/ITO showed the best electrochemical performances. Thus, the optimal assembly layer number of {PDDA–MLC/AuNPs} was three. The electrochemical impedance spectroscopy (EIS) is an effective method for probing the features of surface modified electrode and can provide information on the impedance changes accompanying the stepwise electrode modification process. EIS results of each assembly step are described in Fig. 4C. The electron transfer resistance (R_{ct}) of the bare ITO was estimated to be 434.7 Ω (Fig. 4C, curve i). The R_{ct} of the PDA/ITO increased to 529.7 Ω, which was due to the nonconductive property of PDA, indicating successfully adsorbed of PDA at the surface of the ITO electrode (Fig. 4C, curve j). The semicircle of the {PDDA–MLC/AuNPs}/PDA/ITO was obviously smaller than that of the bare ITO (Fig. 4C, curve k) with the R_{ct} of 94.9 Ω. The semicircle of the {PDDA–MLC/AuNPs}$_2$/PDA/ITO (Fig. 4C, curve l) and the {PDDA–MLC/AuNPs}$_3$/PDA/ITO (Fig. 4C, curve m) were obviously smaller than that of the {PDDA–MLC/AuNPs}/PDA/ITO. The R_{ct} decreased to the {PDDA–MLC/AuNPs}$_2$/PDA/ITO of 54.3 Ω and the {PDDA–MLC/AuNPs}$_3$/PDA/ITO of 30.5 Ω, indicating the promotion of the electron transfer, which was in good agreement with the results of CVs. The biosensor based on three layers of the {PDDA–MLC/AuNPs} got the best electrochemical performances and we used the condition in the following experiments.

UV-vis soret absorption band of Hb may provide the information on the conformational integrity of the protein and the possible denaturation or the conformational change of heme region. As shown in Fig. 5, Hb dissolved in PBS had the Soret band at 405.7 nm (curve a), while in the Hb/{MLC-PDDA/AuNPs}$_3$/PDA film the Soret band appeared at 405.3 nm (curve b). Since the difference of Hb and the Hb/{MLC-PDDA/AuNPs}$_3$/PDA was less than 1 nm, the results showed that Hb in the Hb/{MLC-PDDA/AuNPs}$_3$/PDA had the secondary structure similar to the native state in the solution.

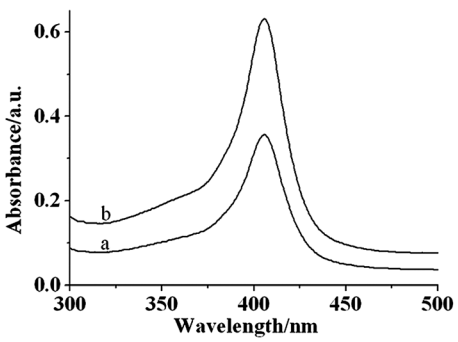

Fig. 5 UV-vis absorption spectra of 0.3 mg mL^{-1} Hb in PBS (a), and the Hb/{PDDA–MLC/AuNPs}$_3$/PDA in PBS (b). The path length: 1 cm.

3.3. Electrochemical characterization of Hb/{MLC-PDDA/AuNPs}$_3$/PDA composite

3.3.1. Direct electrochemistry of Hb. The direct electrochemistry of Hb in the Hb/{MLC-PDDA/AuNPs}$_3$/PDA composite was studied by CV. Fig. 6A showed CVs of the Hb/{MLC-PDDA/AuNPs}$_3$/PDA at the scan rate from 100 to 1000 mV s^{-1} in the N_2-saturated 0.1 M pH 7.0 PBS. The redox process of Hb gave roughly symmetric anodic and cathodic peaks at relatively slow scan rates. When the scan rate increased, the redox potentials (E_{pa} and E_{pc}) of Hb hardly shift. Meanwhile, the redox peak current increased linearly (Fig. 6A inset): $I_{pa} = 1.46 + 9.70 \times 10^{-3}\ v$, $r = 0.9994$; $I_{pc} = -7.50 \times 10^{-1} - 9.50 \times 10^{-3}\ v$, $r = 0.9976$. The formal potential ($E^{0\prime}$) calculated by averaging the cathodic and anodic peak potentials were estimated to be −0.223 V (*vs.* SCE) with 178 mV peak-to-peak separation at the scan rate of 100 mV s^{-1}. All the characteristics suggested that the redox reaction of Hb in the Hb/{MLC-PDDA/AuNPs}$_3$/PDA/ITO was a quasi-reversible surface-controlled electrochemical process. According to the equation of $I_p = n^2F^2vA\Gamma^*/4RT = nFQv/4RT$.[27] n is calculated as 0.86, meaning that one electron transfer is involved. The surface concentration of electroactive

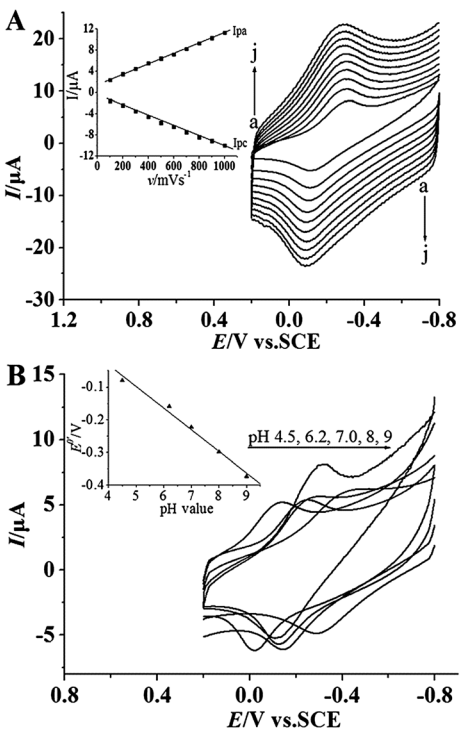

Fig. 6 (A) CVs of the Hb/{PDDA–MLC/AuNPs}$_3$/PDA/ITO in N_2-saturated PBS with different scan rates (from a to j: 100, 150, 200, 250, 300, 350, 400, 450, 500, 600, 700, 800, 900, 1000 mV s^{-1}). Inset: the relationship between cathodic and anodic peak current with scan rate v. (B) Influence of the pH value on the CVs of the Hb/{PDDA–MLC/AuNPs}$_3$/PDA/ITO; pH values (from left to right): 4.5, 6.2, 8.0, 9.0. Inset: the relationship between formal potential and pH. Scan rate: 100 mV s^{-1}.

Γ^* was calculated to be 3.8×10^{-10} mol cm^{-2} from the slope of I_p–v curve. This value was much larger than the theoretical value (1.89×10^{-11} mol cm^{-2}) for the monolayer of Hb on the bare electrode surface, suggesting that the layer-by-layer assembled Hb/{PDDA–MLC/AuNPs}$_3$/PDA/ITO provided a large surface area for enzyme immobilization.

The anodic and cathodic peak potentials were linearly dependent on the logarithm of the scan rates (v) with slopes of $-2.3RT/\alpha nF$ and $2.3RT/(1-\alpha)nF$, respectively.[28] So, the charge-transfer coefficient was calculated as 0.51. The heterogeneous electron transfer rate constant (k_s) was further estimated according to the following equation.[29]

$$log\ k_s = \alpha log\ (1-\alpha) + (1-\alpha)\ log\alpha - log\ (RT/nFv) - (1-\alpha)\ \alpha F\Delta E_p/(2.3RT)$$

Where α is the charge transfer coefficient, and n is the number of electron transfer. R, T and F symbols have their conventional meanings. ΔE_p is the peak to peak potential separation. The calculated k_s was 2.7 s^{-1}, which was much larger than 0.91 s^{-1} of Hb/IL/DNA/PDDA/ITO[17] and 1.2 s^{-1} of Hb-Nafion-GMC/GCE.[29] The result further suggested that the Hb/{PDDA–MLC/AuNPs}$_3$/PDA/ITO can promote the electron transfer between active site of Hb and the electrode surface.

3.3.2. Influence of pH value. The effect of pH value on the direct electrochemistry of Hb at the Hb/{PDDA–MLC/AuNPs}$_3$/PDA/ITO was also investigated. As shown in Fig. 6B, the pH value had an obvious effect on the peak currents of the immobilized Hb. By comparison, the maximum peak current of the immobilized Hb was obtained at pH 7.0. This was due to the neutral pH value close to the physiological environment which could retain activity of the protein effectively.[30]

The peak potentials were also dependent on the pH value. With the increase of pH value from 4.0 to 9.0, the formal potentials ($E^{0\prime}$) shifted linearly to the negative direction (Fig. 6B inset), and the linear regression equation was obtained as $E^{0\prime}$ (mV) = 232.9–66.2 pH, $r = 0.9931$ ($n = 5$) with a slope value of 66.2 mV/pH. The slope value was close to the theoretically expected value of 59 mV/pH at 25 °C, indicating that a single proton transfer accompanied one electron transfer happened in the electrochemical process of Hb at the Hb/{PDDA–MLC/AuNPs}$_3$/PDA/ITO.

3.3.3. Amperometric response of the Hb/{PDDA–MLC/AuNPs}$_3$/PDA/ITO toward H_2O_2. Amperometric detection in electrochemical analysis is a detection method in which the current is proportional to the concentration of the species generating the current. The quantification of H_2O_2 can be achieved *via* the electrochemical detection of the enzymatically liberated Hb.[31] The possible mechanism of electrocatalytic reduction of H_2O_2 at Hb-based electrode has been reported:[32]

$$Hb[Heme(Fe^{3+})] + H_2O_2 \rightarrow \text{Compound I} + H_2O$$

$$\text{Compound I} + H_2O_2 \rightarrow Hb[Heme(Fe^{3+})] + H_2O + O_2$$

$$Hb[Heme(Fe^{3+})] + H^+ + e^- \rightarrow Hb[Heme(Fe^{2+})] \text{ at electrode}$$

$$Hb[Heme(Fe^{2+})] + O_2 \rightarrow Hb[Heme(Fe^{2+})] - O_2 \text{ fast}$$

$$Hb[Heme(Fe^{2+})] - O_2 + H^+ + e^- \rightarrow Hb[Heme(Fe^{3+})] + H_2O \text{ at electrode}$$

The overall reaction would be:

$$H_2O_2 + 2H^+ + 2e^- \rightarrow 2H_2O$$

According to the equations, when H_2O_2 added into the blank PBS, a significant increase in the cathodic (reduction) peak current was observed accompanying the decrease of anodic (oxidation) peak current. The more H_2O_2 added, the greater the reduction peak increased.

Fig. 7 illustrated typical current–time curve of biosensors based on the Hb/{PDDA–MLC/AuNPs}$_3$/PDA/ITO (a), and the Hb/{PDDA–MLC}$_3$/PDA/ITO (b) upon successive addition of different concentrations of H_2O_2 into a 20 mL continuous stirring N_2-saturated 0.1 M pH 7.0 PBS under the optimized experimental condition. −0.22 V was chosen as the working potential, because at such an applied potential, the response of common interference species can be minimized, and the oxygen reduction current can be limited. The current response of the two biosensors increased along with H_2O_2 concentration as mechanism of electrocatalytic reduction of H_2O_2 mentioned above. However, the current changes of the Hb/{PDDA–MLC/AuNPs}$_3$/PDA/ITO were even more obvious than that of Hb/{PDDA–MLC}$_3$/PDA/ITO. As shown in the Fig. 7 insert, the gradient of the linearity based on the Hb/{PDDA–MLC/AuNPs}$_3$/PDA/ITO (a′) much steeper than that of that of Hb/{PDDA–MLC}$_3$/PDA/ITO (b′). All the above indicated that the benign biocompatibility of AuNPs was further improved the performances of the biosensor based on the MLC as the platform.

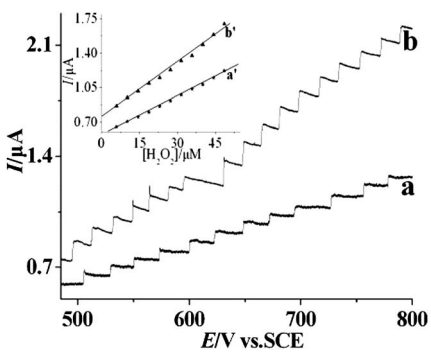

Fig. 7 Amperometric responses of the Hb/{PDDA–MLC/AuNPs}$_3$/PDA/ITO (a) and Hb/{PDDA–MLC/AuNPs}$_3$/PDA/ITO (b) at −0.22 (*vs.* SCE) to successive additions 5.89 μM and 48.5 μM H_2O_2. Inset: The plot of peak current of the Hb/{PDDA–MLC/AuNPs}$_3$/PDA/ITO (a′) and the Hb/{PDDA–MLC}$_3$/PDA/ITO (b′) *vs.* H_2O_2 concentration.

Under the optimized conditions, even with 0.1 μM H_2O_2, obvious amperometric responses were shown (Fig. 8 insert A). The amperometric response of the biosensor showed linearity from 0.03 μM to 1.6 mM (Fig. 8 insert B). The linear regression equation was I_{ss} (μA) = 2.10 × $10^{-2}C$ (μM) + 3.00 × 10^{-1} (n = 34, r = 0.9991) with a detection limit of 0.01 μM (S/N = 3). Comparing with the biosensor fabricated by immobilized multilayer Hb molecules onto three-dimensional gold film electrode[33] and the Hb/nano-Au/L-cysteine (L-cys)/bnano-Au/nano-Pt/CHIT composite film modified platinum disk electrode.[34] Our biosensor based on the Hb/{PDDA–MLC/AuNPs}$_3$/PDA/ITO had a wider linear range. Sun group have intensively studied enzyme-less electrochemical sensors for hydrogen peroxide,[35–40] which have much wider linear range and high detection limit. This advantage achieved the micro and constants determination for H_2O_2 simultaneously. Comparing these H_2O_2 sensors, our proposed biosensor have a much lower detection limit, which was extremely similar with the H_2O_2 biosensor developed by directly grown three–dimensional nanoporous Au networks onto a Ti substrate as a supporting matrix for immobilizing Hb.[41]

The outstanding performance of the biosensor mainly contributed to: (i) The novel structure of the MLC of rough surface with porous structure is beneficial to the stable and effective immobilization of Hb; (ii) the layer-by-layer assembly technology forms unique three dimensionality of the Hb/{PDDA–MLC/AuNPs}$_3$/PDA/ITO. The distinctive shape and properties of the MLC will provide an extraordinary and favorable platform for novel biosensors. The 95% of the steady-state current can be obtained within 2 s by using the biosensor, indicating that a rapid response occurred.

The reproducibility of the Hb/{PDDA–MLC/AuNPs}$_3$/PDA/ITO was investigated, ten enzyme electrodes were made at the same electrode independently showing an acceptable repeatability for the current detected at 5 μM H_2O_2. The stability and repeatability of the biosensor were studied in the linear range of H_2O_2. The relative standard deviation was 2.7% for seven successive measurements of 130.0 μM H_2O_2 in N_2–saturated 0.1 M pH 7.0 PBS, indicating that the proposed biosensor possessed good repeatability. The CV responses of the biosensor in N_2–saturated 0.1 M pH 7.0 PBS showed no obvious change after 25 cycles and then decreased slowly with the increase of the cycle, suggesting that the biosensor was stable. The storage stability of the biosensor was further investigated. The cathodic peak current of the Hb/{PDDA–MLC/AuNPs}$_3$/PDA/ITO was measured using the same electrode and it retained above 95% of its initial response stored at 4 °C after 4 weeks. These results displayed that the biosensor based on the Hb/{PDDA–MLC/AuNPs}$_3$/PDA/ITO had a good reproducibility and stability.

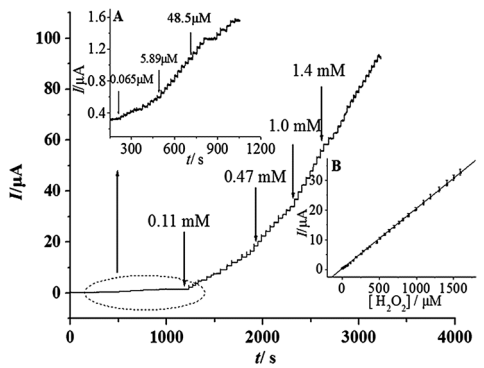

Fig. 8 Amperometric responses of the Hb/{PDDA–MLC/AuNPs}$_3$/PDA/ITO at −0.22 (*vs.* SCE) upon successive addition of 0.11 mM, 0.47 mM, 1.0 mM and 1.4 mM H_2O_2 in N_2–saturated PBS. Inset: (A) The amperometric response of the Hb/{PDDA–MLC/AuNPs}$_3$/PDA/ITO to successive additions of 0.065 μM, 5.89 μM and 48.5 μM H_2O_2; (B) plot of peak current *vs.* H_2O_2 concentration.

4. Conclusions

By controlling the initiator amount of Fc and reaction temperature of hydrothermal reactions, a new kind of carbon nanomaterial with the morphology of the plant monkshoodvine root-bark was achieved. Electrochemical studies showed that the MLC can accelerate the direct electron transfer of Hb through layer-by-layer assembly of Hb and the MLC. Based on the excellent electrocatalytic ability of the Hb/{PDDA–MLC/AuNPs}$_3$/PDA/ITO for H_2O_2 reduction, a novel H_2O_2 biosensor was presented. The prepared H_2O_2 biosensor not only exhibited excellent electrocatalytic ability towards H_2O_2, but also exhibited fast response and wide linear range. The reason can be ascribed to that of the MLC with porous construction greatly enlarging the specific surface to effectively increase the amount of Hb immobilized. The present study may pave the way for the synthesis of novel nanomaterials with unique morphology and properties, which will be employed to design novel electrochemical biosensor with other bio-systems. Further works derived by employing the MLC as the platform of biosensors are on our schedule.

Acknowledgements

The authors appreciate the financial support from the National Natural Science Foundation of China (No.20875076), the Scientific Initializing Foundation of Northwest University (No. PR09036), the Science Foundation of Northwest University (No.09NW02), the Education Department of Shaanxi Province, China (No. 2010JK877) and the NWU Doctorate Dissertation of Excellence Funds (No. 08YYB06).

Notes and references

1 M. Zhao, X. M. Wu and C. X. Cai, *J Phys Chem C*, 2009, **113**, 4987–4996.
2 A. J. Qureshi, W. P. Kang, J. L. Davidson and Y. Gurbuz, *Diamond Relat Mater.*, 2009, **18**, 1401–1420.
3 S. Iijima, *Nature*, 1991, **354**, 56–58.
4 Y. Lu, Z. P. Zhu, D. S. Su, D. Wang, Z. Y. Liu and R. Schlögl, *Carbon*, 2004, **42**, 3199–3207.
5 J. J. Vilatela and A. H. Windle, *Adv Mater.*, 2010, **22**, 4959–4963.
6 P. L. Kuo, C. H. Hsu, W. T. Li, J. Y. Jhan and W. F. Chen, *J Power Sources.*, 2010, **195**, 7983–7990.
7 S. Y. Zhu and G. B. Xu, *Nanoscale*, 2010, **2**, 2538–2549.
8 M. Ohtani, K. Saito and S. Fukuzumi, *Chem Eur J.*, 2009, **15**, 9160–9168.
9 K. Y. Yan, Q. Z. Xue, D. Xia, H. J. Chen, J. Xie and M. D. Dong, *ACSnano*, 2009, **3**, 2235–2240.
10 X. B. Lu, J. H. Zhou, W. Lu, Q. Liu and J. H. Li, *Biosens Bioelectron.*, 2008, **23**, 1236–1243.
11 X. B. Lu, Y. Xiao, Z. B. Lei, J. P. Chen, H. J. Zhang, Y. W. Ni and Q. Zhang, *J Mater Chem.*, 2009, **19**, 4707–4714.

12 C. S. Shan, H. F. Yang, J. F. Song, D. X. Han, A. Ivaska and L. Niu, *Anal Chem.*, 2009, **81**, 2378–2382.
13 K. F. Zhou, Y. H. Zhu, X. L. Yang, J. Luo, C. Z. Li and S. R. Luan, *Electrochim Acta*, 2010, **55**, 3055–3060.
14 X. R. Liu, Y. Li, J. B. Zheng, J. C. Zhang and Q. L. Sheng, *Talanta*, 2010, **81**, 1619–1624.
15 Y. H. Xiao and C. M. Li, *Electroanal*, 2008, **20**, 648–662.
16 Q. L. Sheng and J. B. Zheng, *Biosens Bioelectron.*, 2009, **24**, 1621–1628.
17 R. F. Gao, J. B. Zheng and L. F. Qiao, *Electroanal.*, 2010, **22**, 1084–1089.
18 X. Y. Liu, X. D. Zeng, N. N. Mai, Y. Liu, B. Kong, Y. H. Li, W. Z. We and S. L. Luo, *Biosens Bioelectron.*, 2010, **25**, 2675–2679.
19 J. M. Pingarrón, P. Y. Sedeño and A. G. Cortés, *Electrochim. Acta.*, 2008, **53**, 5848–5866.
20 D. Y. Tang, B. Y. Xia and Y. Q. Zhang, *Microchim Acta.*, 2008, **160**, 367–374.
21 Z. H. Guo, Y. Shen, M. K. Wang, F. Zhao and S. J. Dong, *Anal. Chem.*, 2004, **76**, 184–191.
22 B. V. Enustun and J. J. Turkevich, *J Am Chem Soc.*, 1963, **85**, 3317.
23 Z. P. Liu, X. F. Zhou and Y. T. Qian, *Adv Mater.*, 2010, **22**, 1963–1966.
24 S. Liu, J. Q. Tian, L. Wang, Y. L. Luo, J. F. Zhai and X. P. Sun, *J Mater Chem.*, 2011, **21**, 11726–11729.
25 V. O. Nyamori and N. J. Coville, *Organometallics*, 2007, **26**, 4083–4085.
26 J. M. Shen, L. Xu, Y. G. Liu, C. L. Lu, W. H. Hou and J. J. Zhu, *Chem Mater.*, 2008, **20**, 3034–3041.
27 E. Laviron, *J Electroanal Chem.*, 1979, **100**, 263–270.
28 X. J. Zhao, Z. B. Mai, X. H. Kang, Z. Dai and X. Y. Zou, *Electrochim Acta*, 2008, **53**, 4732–4739.
29 X. B. Lu, Y. Xiao, Z. B. Lei and J. P. Chen, *Biosens Bioelectron.*, 2009, **25**, 244–247.
30 Z. Dai, Y. Xiao, X. Z. Yu, Z. B. Mai, X. J. Zhao and X. Y. Zou, *Biosens Bioelectron.*, 2009, **24**, 1629–1634.
31 Y. Liu, Q. Y. Jiang, S. Y. Lu, Y. Zhang and H. Y. Gu, *Appl. Biochem. Biotechnol.*, 2009, **152**, 418–427.
32 X. B. Lu, H. J. Zhang and Y. W. Ni, *Biosens. Bioelectron.*, 2008, **24**, 93–98.
33 Y. Chen, X. J. Yang, L. R. Guo, J. Li, X. H. Xia and L. M. Zheng, *Anal. Chim. Acta*, 2009, **644**, 83–89.
34 G. Yang, R. Yuan and Y. Q. Chai, *Colloids Surf., B*, 2008, **61**, 93–100.
35 S. Liu, J. Q. Tian, J. F. Zhai, L. Wang, W. B. Lu and X. P. Sun, *Analyst*, 2011, **136**, 2037–2039.
36 S. Liu, J. Q. Tian, L. Wang, H. L. Li, Y. W. Zhang and X. P. Sun, *Macromolecules*, 2010, **43**, 10078–10083.
37 S. Liu, L. Wang, J. Q. Tian, Y. L. Luo, X. X. Zhang and X. P. Sun, *J. Colloid Interface Sci.*, 2011, **363**, 615–619.
38 G. H. Chang, Y. L. Luo, W. B. Lu, F. Liao and X. P. Sun, *J. Nanopart. Res.*, 2011, **13**, 2689–2695.
39 S. Liu, J. Q. Tian, L. Wang and X. P. Sun, *Carbon*, 2011, **49**, 3158–3164.
40 W. B. Lu, Y. L. Luo, G. H. Chang and X. p. Sun, *Biosens. Bioelectron.*, 2011, **26**, 4791–4797.
41 A. K. M. Kafi, A. Ahmadalinezhad, J. P. Wang, D. F. Thomas and A. C. Chen, *Biosens. Bioelectron.*, 2010, **25**, 2458–2463.

